Properties of plasmoids observed in Saturn's dayside and nightside magnetodisc

Y. Xu[1], R. L. Guo[2], Z. H. Yao[1,3]*, D. X. Pan[1], W. R. Dunn[4], S.-Y. Ye[5], B. Zhang[6], Y. X. Sun[7], Y. Wei[1] and A. J. Coates[4]

1 Key Laboratory of Earth and Planetary Physics, Institute of Geology and Geophysics, Chinese Academy of Sciences, Beijing, China

2 Laboratory for Planetary and Atmospheric Physics, STAR institute, Université de Liège, Liège, Belgium

3 College of Earth and Planetary Sciences, University of Chinese Academy of Sciences, Beijing, China

4 UCL Mullard Space Science Laboratory, Dorking, UK

5 Department of Earth and Space Sciences, Southern University of Science and Technology (SUSTech), Shenzhen, China

6 Department of Earth Sciences, the University of Hong Kong, Pokfulam, Hong Kong SAR, China

7 Institute of Space Physics and Applied Technology, School of Earth and Space Sciences, Peking University, Beijing, China

Corresponding author: Zhonghua Yao (z.yao@ucl.ac.uk)

Key points:

- This study reveals the existence of plasmoids in Saturn's dayside magnetodisc.
- A global local time distributions of plasma properties in plasmoid is obtained.
- We infer the evolution of plasmoid during rotation from electron density distribution.

Abstract

Plasmoid is a key process for transferring magnetic flux and plasma in planetary magnetospheres. At Earth，plasmoid is a key media transferring energy and mass in the "Dungey Cycle" magnetospheric circulation. For giant planets, plasmoid is primarily generated by the dynamic processes associated with “Vasyliunas Cycle”. It is generally believed that planetary magnetotails are favourable for producing plasmoids. Nevertheless, recent study reveals that magnetic field lines could be sufficiently stretched to allow magnetic reconnection (Guo et al. 2018a) in Saturn’s dayside magnetodisc. And in the study, we report direct observations of plasmoid in Saturn’s dayside magnetodisc. Moreover, we perform a statistical investigation on the global plasmoid electron density distribution. The results show an inverse correlation between the nightside plasmoid electron density and local time, and the maximum plasmoid electron density around prenoon local time on the dayside. These results are consistent with the magnetospheric circulation picture associated with"Vasyliunas Cycle".

Plain Language Summary

Plamoid is a crucial structure to transfer mass and energy in a planetary magnetosphere. It is known that magnetic field lines are stretched in nightside tail, and more dipolar in dayside at the Earth. Similar configuration is also applied to the giant planets Saturn and Jupiter. Therefore, besides the magnetopause, the reconnection, dipolarizaiton and plasmoids are only expected to exist in nightside tail. However, recent studies reveal that the magnetic field lines in Saturn’s dayside magnetodisc are more stretched than previously expected and could trigger magnetic reconnection in dayside disc. Since plasmoids are closely related to reconnection, it is natural to expect plasmoids in Saturn’s dayside disc. Using the Cassini dataset, we directly confirm the existence of plasmoid in Saturn’s dayside disc. The plasma density shows a nice decreasing trend from dusk to dawn, which is consistent with the Vasyliunas cycle picture.

1. Introduction

Plasmoid, also known as flux rope, is a fundamental element in transporting magnetic flux and mass at the Earth (Machida et al.,2000), Mercury (DiBraccio et al. 2015) and giant planets (Vogt et al.,2014). It is often believed that magnetic reconnection is a key driver for plasmoid (Slavin et al., 2003). Plasmoid was first identified at Earth’s magnetopause by the ISEE 1 and 2 spacecraft (Russell and Elphic, 1978, 1979). In the near-Earth magnetotail, the result of X-type reconnection is suggested to generate the tailward-moving large loop-like magnetic structure(Hones, 1979). Recent investigations show that magnetic reconnection could take place in the near-Earth magnetotail (Angelopoulos et. al 2019).

Plasmoids/flux ropes (FRs) are considered to be an important consequence of astrophysical and space plasma eruptions, e.g., during solar coronal mass ejection (CME) (Vourlidas et al. 2013). The bipolar perturbation in north-south magnetic component (Bz) in a two dimensional picture is widely adopted as an identifier of plasmoid/FR events in previous literatures (e.g., Ieda et al., 1998; Slavin et al., 2003; Zong et al., 2004, etc.). Plasmoids are often accompanied with high-speed plasma flows that are associated with energetic ions and electrons

(Slavin et al., 2003). At Earth, the typical duration of plasmoid/FR is about two minutes (Ieda et al., 1998), showing increased electron density and accelerated population (Chen et al., 2008).

Besides Earth, magnetic reconnection and plasmoids are also identified in the magnetopauses and magnetotails of Jupiter and Saturn, playing important roles in driving magnetospheric processes in their space environments (Huddleston et al., 1997; Badman et al. 2013; Arridge et al.2016; Masters 2017). Magnetic reconnection processes may be different between Earth and giant planets. For example, magnetic reconnection in Saturn's magnetotail could last for about 19 hours (Arridge et al. 2016), which is much longer than the reconnection processes in terrestrial magnetotail. The different features of magnetic reconnection may result in different characteristics of other associated processes (e.g., plasmoid) between the two planets. Unlike the terrestrial magnetosphere that is mostly driven by solar wind, the magnetospheric processes at giant planets are driven by both the solar wind and internal sources (i.e., their moon activities). The plasma and magnetic flux circulations driven by solar wind are often known as Dungey cycle (Dungey, 1961), while the internally driven circulations are often known as "Vasyliunas Cycle" (Vasyliunas,1983). Plasmoids/FRs are considered to play an important role on the magnetic flux closure in the nightside of Saturn's magnetosphere (Jackman et al. 2011; Arridge et al. 2016). Jackman et al. (2011) indicate that plasmoids/FRs at Saturn are typically about 8 min in duration.

At Saturn and Jupiter, the internal sources are strongly influenced by planetary rotation , which are expelled outward by the large centrifugal force. Accompanying this process, the magnetic field lines are also stretched in all local times of the magnetodisc (Kivelson and Southwood, 2005). Thus, magnetodisc at Saturn may potentially allow magnetic reconnection in dayside sectors. By analyzing the large magnetic field dataset from Cassini magnetometer (Dougherty et al. 2004), Delamere et al. (2015) proposed drizzle-like reconnection in Saturn's magnetodisc, including the dayside sectors. In a later study, Yao et al. (2017) reveal that magnetic reconnection site may corotate with Saturn, and thus suggest that reconnection site could exist in all local times including the dayside magnetodisc. Guo et al.(2018a) show direct evidence of magnetic reconnection in Saturn's dayside magnetodisc by analyzing high-resolution electron distributions and magnetic field from Cassini dataset (Dougherty et al. 2004; Young et al. 2004). Since plasmoid/FR, magnetic reconnection and magnetic dipolarization are closely associated plasma processes in planetary magnetospheres, it is natural to expect plasmoids to exist in Saturn's dayside magnetodisc. The evolution and formation of plasmoids at giant planets are also vital in understanding the energy coupling processes (e.g., Jackman et al., 2008; Delamere et al., 2015; Jasinski et al., 2019), while all these studies are based on cases from the nightside magnetotail. It is unknown whether the dayside magnetodisc would produce plasmoids. If so, the evolution of plasmoids during rotation would provide crucial information for understanding plasma and magnetic flux circulation in giant planets.

In this study, we report for the first time plasmoid structures in Saturn's dayside magnetodisc. The associated energetic particle features are also investigated. Moreover, we survey the Cassini dataset for plasmoid cases on both dayside and nightside, and infer a global evolving picture by comparing the properties of events at different local times.

2. Observations

The magnetic field data in this study is from the Cassini MAG instrument (Dougherty et al. 2004). Thermal ion and electron measurements are provided by the Cassini-CAPS/IMS/ELS

(Young et al. 2004), with energy range up to 28 keV for electrons and up to 50 keV for ions. Moreover, we utilize energetic particle data from the Low-Energy Magnetospheric Measurements System (LEMMS) and the Ion and Neutral Camera (INCA) of the Magnetosphere Imaging Instrument (MIMI) (Krimigis et al. 2004), which provide the coverage of energy range from 18 keV to 832keV for electrons, and from 27 keV to 3930 keV for ions. Combining the in-situ magnetic field and particle data, we could obtain pitch angle information for hot electrons, although the angular coverage is limited due to instrumental issues.

2.1 A case study on September 21, 2008

Figure 1 shows observations of a plasmoid event on September 21, 2008 between 17:20 UT and 19:00 UT, during which Cassini was at a radial distance of ~20.2 R_s (Saturn's Radius, $1R_s$ = 60268 km) from Saturn's center and the local time (LT) is 10.8. Figure 1a shows the magnetic components in Kronographic Radial–Theta–Phi coordinates (a spherical coordinate system in which Z-axis represents Saturn's rotation axis, pointing north). Figure 1b shows the magnetic field components in the reconnection X-line coordinate system (Arridge et al. 2016; Guo et al. 2018). This is a rectangular coordinate system, which could largely eliminate the bend-back effect of the magnetic field lines in the magnetodisc. Figure 1c shows the differential fluxes of electron with energies from 18 to 832 keV measured by the MIMI-LEMMS instrument. The energy spectrogram of omnidirectional hot-electron flux measured by the CAPS-ELS instrument is shown by Figure 1d. Figures 1(e-g) show the pitch angle distribution of electrons in four different energy ranges which is from 200eV to 500eV, 500eV to 3keV and 3keV to 30keV (due to the limited field of view of the instrument, the coverage of pitch angles is very poor during the whole period, which is a common situation in Cassini CAPS-ELS data set). The electron density obtained by CAPS-ELS instrument is shown in Figure 1h. Figure 1i shows the differential flux of the energetic ions (mainly protons) in the range of 27 keV to 4 MeV from the MIMI-LEMMS instrument. Figure 1j shows the energy spectrogram for omnidirectional ion flux measured by the CAPS-IMS instrument.

As indicated by the bipolar variation of B_θ at ~18 UT (marked by the colored shadow), a plasmoid event was detected by Cassini in the prenoon sector (at ~10.8 Local Hour). The magnetic field in reconnection coordinate system (Figure 1b) show that Bx is dominant before the perturbation at 17:55 UT, indicating that the spacecraft was located in the outer layer of the current sheet. In Figure 1a, we can see that before 17:55 UT, the three components of the magnetic field are in a rather quiet state. From 17:55 UT, B_θ component experienced a steep drop (down to - 2.5nT) and a rapid rise to above 0 nT, and then gradually recovered to increase, until it reached the local maximum at 18:09. Six minutes later, B_θ is restored to a relatively quiet state. During the bipolar magnetic variation, the electron and ion spectrograms (Figure 1(d, j)) are featured by higher than ambient plasma energies (electron in the energy range of 100eV ~ 10KeV, and ion in the energy range of 1keV ~ 10keV). Higher energetic electron and ion fluxes in the period were also clearly seen in Figure 1(c,i). Based on the variation of B_θ that has a peak at 18:09, we divide the event into two stages, as highlighted in blue and red. In stage 1, the electron pitch-angle distribution is isotropic (as shown in Fig. 1(e~g)), when sharp increases in electron and ion flux (as shown in Fig. 1i) were detected. Compared with this, the electron pitch-angle distribution of stage 2 is field-aligned. And the peaks of electron and ion fluxes were detected in stage 2, which were slightly lower than those in stage 1. During the whole period, the electron density is clearly higher than that in the background environment, especially in stage 1(as shown in Fig. 1h), which is expected when the spacecraft travelled from outer plasmasheet

to the central region as indicated by the decreasing Br. It is also possible that the plasma density is higher in a plasmoid structure.

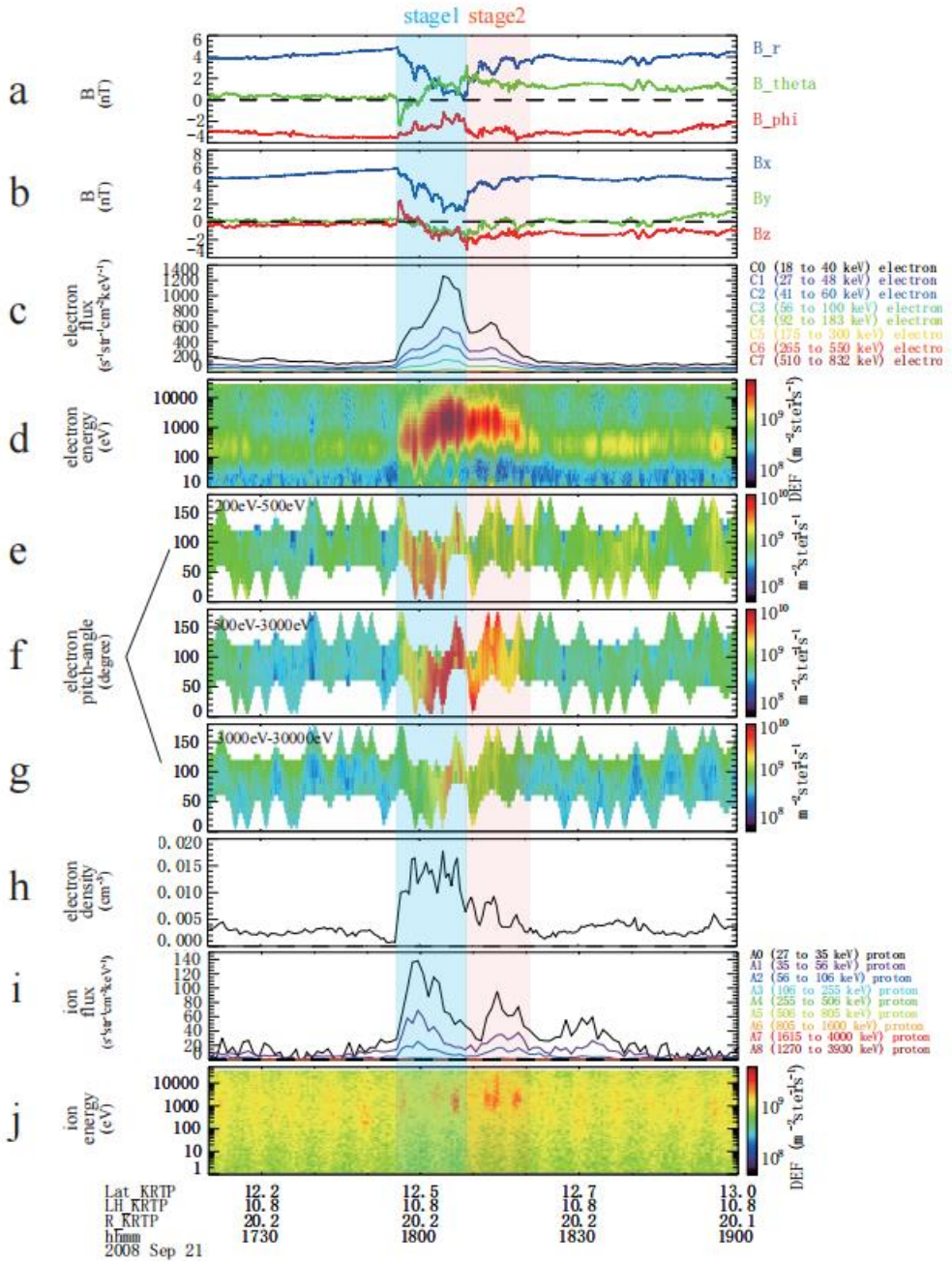

Figure 1. A dayside plasmoid event on September 21, 2008. (a) Three magnetic field components in KRTP coordinates, and (b) in reconnection coordinate. (c) Energetic electron differential flux from MIMI-LEMMS. (d) Energy spectrogram of omnidirectional electron flux from CAPS-ELS. (e)-(g) Pitch angle distribution for electrons within energy ranges of 200 eV to 500 eV, 500 eV to 3 keV, and 3 keV to 30 keV. (h) Electron density from CAPS-ELS. (i) Energetic proton differential flux from IMI-LEMMS. (j) Energy spectrogram for omnidirectional ion flux from CAPS-IMS. We divide this event into two stages according to the different magnetic field and plasma properties, which are highlighted by blue and red.

2.2 A statistical investigation of plasmoid events

To perform a statistical investitation, we surveyed the Cassini dataset from 2005 to 2010. The negative B_θ component is usually considered as an identifier of plasmoid. In the selection of event, we require B_θ to reach a certain negative value. Futhermore, plasmoid events are often featured by a sharp drop of B_θ component, thus dB_θ/dt is used to restrict our event selection. Considering the complexity of magnetic perturbations in magnetosheath region that may affect the analysis of plasmoid features, we require a relatively quiet background of magnetic field prior to the selection of plasmoid events. The quiet background is defined by a small standard deviation of the B_θ component of the background magnetic field. The plasma temperature is an additional parameter to exclude the influence of the magnetosheath region. Considering the great influence and disturbance caused by cold plasma in the inner magnetosphere, we only focus on the events beyond 15 R_S , where the hot plasma dominates. Based on the above considerations, we determine the selection criteria of plasmoid starting time as below.

(1) dB_θ/dt has a negative growth of at least - 0.3nT/min at the event (We take the magnetic field data with one-minute accuracy, so this condition is equivalent to the negative growth of - 0.3nT for ΔB_θ in one minute);

(2) The minimum value of B_θ within 3 minutes after the beginning is less than - 0.5nT;

(3) The standard deviation of B_θ from 25 min to 10 min before the event is less than 1.5 nT;

(4) The location of each event is requested to be more than $15R_S$ away from Saturn (in order to study the concentration properties of Saturn in the noon sector, the definition of the dayside event in this paper is 8-16h local time, and the rest is called the nightside.);

(5) The maximum electron temperature within 5 minutes before and after the event beginning is not less than 90 eV.

We define the start time of a plasmoid event as the time when dB_θ/dt first reaches - 0.3nT. And the end time is selected when B_θ reaches the first local maximum value (defined as the maximum value within 5 minutes before and after) which is larger than 0 after recovering from the negative value. It should be noted that the magnetopause is a boundary caused by the continuous interaction between the magneotsheath and the magnetosphere, so that the perturbations of magnetic field and particles are persistent. To avoid potential confusions, we do not select the events in the magnetopause boundary layer in this study. Therefore, we manually exclude the remaining few events that are not plasmoid events.

Applying the above event selection criteria, we have finally identified 116 plasmoid events (65 on the dayside and 51 on the nightside) from 2005 to 2010. Magnetic perturbations due to Titan flyby are excluded in this study. A time list of events and a record of each select criterion are shown in the supplementary material. We calculate the average of the electron density data from the start time to the end time for each plasmoid event.

Panel a and panel b of Figure 2 show the global distribution of dayside and nightside electron density respectively. The trajectory of the spacecraft is also overlayed on the diagram. Panel c shows the distribution of the ratio of dayside and nightside plasmoid electron density to

background density (background electron density is defined as the average electron density of the 25 minutes to 10 minutes ahead of the event). In the dayside, we can see in Figure 2a that plasmoid events are mainly concentrated in local times between 10 LT and 14 LT (this may be related to the orbital distribution of Cassini), and a bunch of high electron density events appear at ~ 11 LT. When at other local time, the event electron density is generally low. In the nightside (as shown in Figure 2b), the plasmoid events are concentrated in three local times (~ 21LT, ~ 1LT, ~ 5LT). We can qualitatively see the inverse correlation of electron density with radial distance and local time on the nightside. We note that the plasmoid events are not equally distributed on all orbits. This is probably because that different orbits were during different solar wind conditions, which may strongly influence the occurrence of plasmoid. For example, in September 2006, 14 plasmoid events are identified successively. Panel c of Figure 2 shows the global distribution of the ratio of electron density to the background density of plasmoid events. It is obvious that electron density for the majority of the events is higher than the background density. 80/116 events show higher density than their background, in which 42/65 events were on the dayside and 38/51 events were on the nightside. The electron density inside the plasmoid is larger than the background density in a considerable number of cases, which is similar to the magnetic island on Earth (Chen et al., 2008).

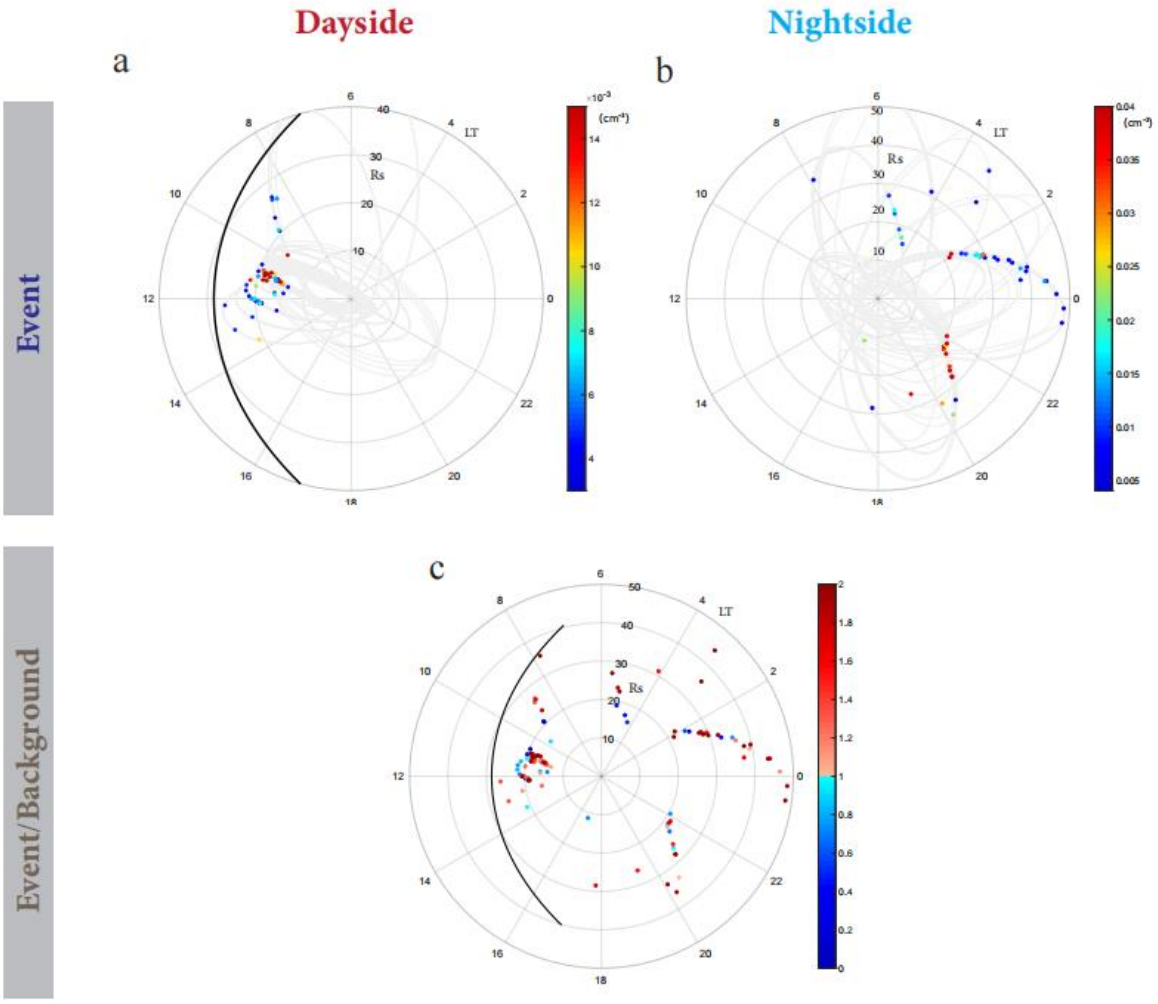

Figure 2. The distribution of plasmoid electron density. Panel (a,b) shows the global distribution of dayside and nightside electron density respectively. The trajectory of the aircraft is also superimposed on the diagram. Panel c below shows the ratio of the dayside and nightside plasmoid electron density to the background density. Magnetopause location (the black curve) predicted using the A60 model (Kanani et al., 2010) with improved parameters, while the solar wind dynamic pressure is estimated using the Tao model (Tao et al., 2005) (PSW=0.00606nP).

Figure 3a shows the distribution of electron density at different local times on the dayside, where the red dots represent the plasmoid events of R < $20R_s$, and the blue dots represent the plasmoid events of R > $20R_s$. The electron density has a significant peak at LT~11 when R< $20R_s$. It can be clearly seen from Figure 3a that most of the events (7 in 8 events) with electron density greater than 0.015 (cm^{-3}) are concentrated in the 11 LT region, including most high-density events. The median numbers for two selected sectors, 10:30-11:30 LT and 11:30-12:30 LT, are 0.01028 (cm^{-3}) and 0.00499 (cm^{-3}) shown by the blue squares. We note that Delamere et al. (2015) also show peak occurrence of drizzle-like reconnection events at ~11 LT, which is probably related to the electron density peak of plasmoids in this study. Figure 3b shows the distribution of the electron density at different radial distances for dayside sectors. Similar to Figure 3a, we show the medians of three selected intervals with radial distance in 15-17R_s, 17-19R_s and 19-21R_s, which are 0.00652 (cm^{-3}), 0.01147 (cm^{-3}) and 0.00629 (cm^{-3}). The peak electron density is near 18R_s. Figure 3c shows the electron density distribution at different local times for nightside sectors, where the red dots represent the plasmoid events of R < 30R_s and the blue dots represent the plasmoid events of R > 30R_s. We see the inverse correlation between the electron density and the local time from the dusk-side to the dawn-side. We fitted data when R < 30R_s, R > 30R_s and total events respectively. The results are obvious: from the dusk-side to the dawn-side via midnight, the electron density of plasmoid decreased gradually. The results are consistent with the picture of “Vasyliunas Cycle”, during which the magnetic flux tube expands radially during the cycle in the nightside, resulting in a significant decrease of its electron density. Figure 3d shows the relation between the electron density on the nightside and the radial distance. The fitting results are consistent with common sense – the electron density generally decreases towards larger distances.

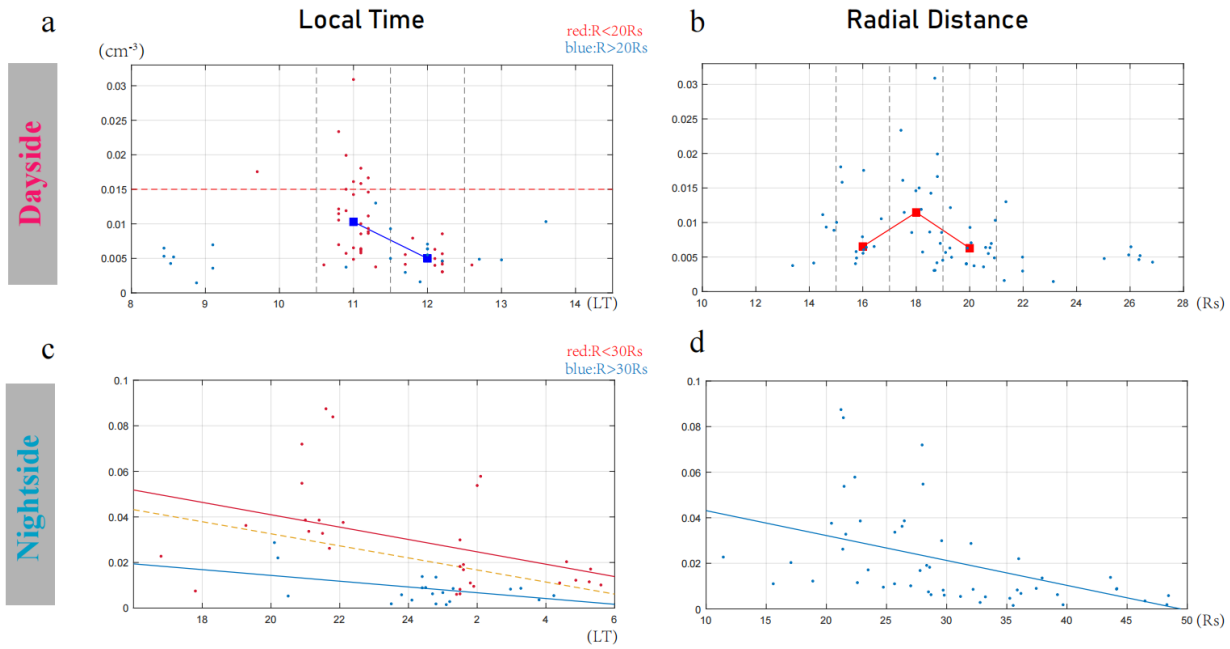

Figure 3. Plasmoid electron density statistical results. (a) The distribution of the electron density at different local times in dayside sectors; (b) The distribution of the electron density at different radial distances in dayside sectors; (c) The distribution of the electron density at different local times of nightside. The equation of red fitting line is $y = -0.00271x + 0.0952$, correlation coefficient R^2 = 0.176, SSE, the sum of squares due to error is 0.0126; blue line fitting equation is $y = -0.00127x + 0.0397$, R^2 = 0.260, SSE = 6.74×10^{-4}; yellow line equation is $y = -0.00265x + 0.0855$, R^2 = 0.166 , SSE = 0.0183 ; blue line fitting equation is y = -0.00168 x + 0.0496, R^2 = 0.302 , SSE = 0.000627; (d) The distribution of the electron density at different radial distances of nightside. The fitting equation is y = -0.00109x + 0.0541, R^2 = 0.235, SSE = 0.0168.

3. Discussion and Conclusion

Plamsa circulation in planetary magnetosphere is a key topic in space physics community. At the Earth, the circulation of mass and energy is driven by solar wind, known as Dungey Cycle. While at giant planets like Saturn and Jupiter, whose magnetospheres rapidly rotate, the mass circulation is dominated by Vasyliunas cycle (Vasyliunas, 1983). In addition, the reconnection processes which cause the formation of plasmoid are suggested to be small-scale and "drizzle-like" (Delamere et al. 2015; Guo et al. 2018b), meaning that plasmoids can be generated at all local times. At different local times, plasmoids show different properties constrained by different conditions. At near-noon local times, the flux tube is compressed to have a minimum volume due to the magnetopause. From the dusk-side to the dawn-side, the flux tube would gradually expand. In adiabatic condition, flux tube expansion would lead to decease of electron density, thus we would expect a continuous decrease of electron density from the dusk-side to the dawn-side, and the maximum of electron density near noon. The statistical results are consistent with the expectation from Vasyliunas cycle. Figure 4 is a cartoon to illustrate the evolution of plasmoid and flux tube during Vasyliunas cycle.

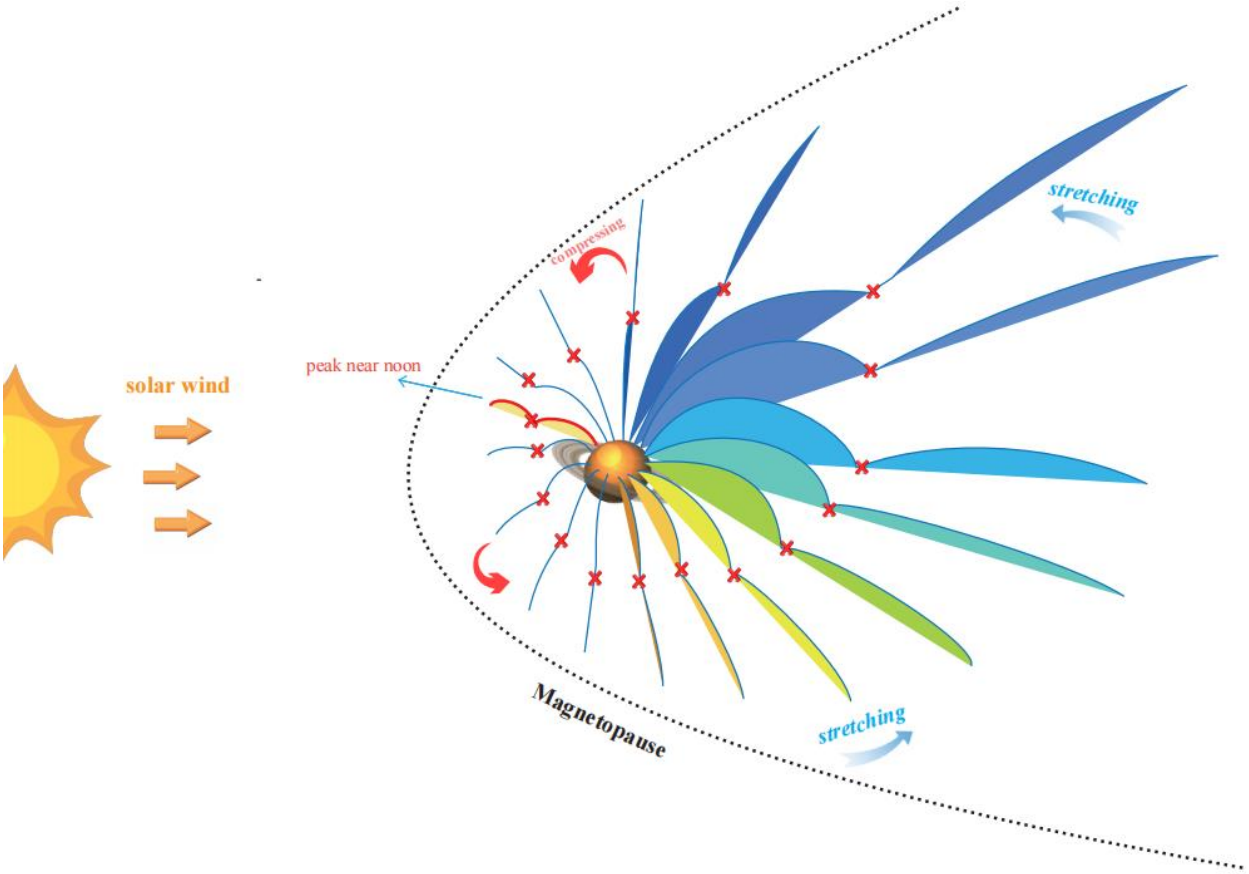

Figure 4. Physical images of the "Vasyliunas Cycle" in the magnetosphere of Saturn. The filled color indicates the relative electron density. On the dayside, a peak of electron density is observed near noon.

The main results are summarized as below,

(1) For the first time, plasmoid structures are shown in dayside planetary magnetodisc. As plasmoid is a crucial media to carry mass and energy, the dayside magnetodisc plasmoid would provide important implications for understanding planetary mass and energy circulations.

(2) As shown by the local time distribution of plasma properties of plasmoids, electron density shows a peak at ~ 11 LT, and a generally decreasing trend from dusk to dawn via midnight.

(3) The evolution of plasmoid electron density is consistent with the flux tube evolving picture in Vasyliunas cycle.

Acknowledgments: The Cassini data presented in this study are available at https://pds-ppi.igpp.ucla.edu/search/?t=Saturn&sc=Cassini&facet=SPACECRAFT_NAME&depth=1 via MAG, CAPS and MIMI instruments. This work was supported by the Strategic Priority Research Program of Chinese Academy of Sciences，Grant No. XDB 41000000, the National Science Foundation of China (grant 42074211) and Key Research Program of the Institute of Geology & Geophysics CAS (grant IGGCAS-201904). The authors wish to thank the International Space Science Institute in Beijing (ISSI-BJ) for supporting and hosting the meetings of the International Team on "The morphology of auroras at Earth and giant planets: characteristics and their magnetospheric implications", during which the discussions leading/contributing to this publication were held.

References

Angelopoulos, V., Artemyev, A., Phan, T. D., & Miyashita, Y. J. N. p. (2020). Near-Earth magnetotail reconnection powers space storms. 16(3), 317-321.

Arridge, C. S., Eastwood, J. P., Jackman, C. M., Poh, G. K., Slavin, J. A., Thomsen, M. F., . . . Dougherty, M. K. (2015). Cassini in situ observations of long-duration magnetic reconnection in Saturn's magnetotail. Nature Physics, 12(3), 268-271. doi:10.1038/nphys3565.

Badman, S. V., Masters, A., Hasegawa, H., Fujimoto, M., Radioti, A., Grodent, D., . . . Coates, A. J. (2013). Bursty magnetic reconnection at Saturn's magnetopause. Geophysical Research Letters, 40(6), 1027-1031. doi:10.1002/grl.50199.

Bagenal, F., Wilson, R. J., Siler, S., Paterson, W. R., & Kurth, W. S. (2016). Survey of Galileo plasma observations in Jupiter's plasma sheet. Journal of Geophysical Research (Planets), 121, 871-894. doi:10.1002/2016JE005009.

Chen, L. J., Bhattacharjee, A., Puhl-Quinn, P. A., Yang, H., Bessho, N., Imada, S., . . . Georgescu, E. (2007). Observation of energetic electrons within magnetic islands. Nature Physics, 4(1), 19-23. doi:10.1038/nphys777.

Delamere, P. A., Otto, A., Ma, X., Bagenal, F., & Wilson, R. J. (2015). Magnetic flux circulation in the rotationally driven giant magnetospheres. Journal of Geophysical Research: Space Physics, 120(6), 4229-4245. doi:10.1002/2015ja021036.

DiBraccio, G. A., Slavin, J. A., Imber, S. M., Gershman, D. J., Raines, J. M., Jackman, C. M., . . . Science, S. (2015). MESSENGER observations of flux ropes in Mercury's magnetotail. 115, 77-89.

Dougherty, M., Kellock, S., Southwood, D., Balogh, A., Smith, E., Tsurutani, B., . . . Russell, C. J. T. c.-h. m. (2004). The Cassini magnetic field investigation. 331-383.

Dungey, J. W. (1961). Interplanetary Magnetic Field and the Auroral Zones. Physical Review Letters, 6(2), 47-48. doi:10.1103/PhysRevLett.6.47.

Guo, R. L., Yao, Z. H., Wei, Y., Ray, L. C., Rae, I. J., Arridge, C. S., . . . Dougherty, M. K. (2018). Rotationally driven magnetic reconnection in Saturn's dayside. Nature Astronomy, 2(8), 640-645. doi:10.1038/s41550-018-0461-9.

Hones, E. W. (1979). Transient phenomena in the magnetotail and their relation to substorms. Space Science Reviews, 23(3), 393-410. doi:10.1007/BF00172247.

Huddleston, D. E., Russell, C. T., Le, G., & Szabo, A. (1997). Magnetopause structure and the role of reconnection at the outer planets. Journal of Geophysical Research: Space Physics, 102(A11), 24289-24302. doi:10.1029/97ja02416.

Ieda, A., Machida, S., Mukai, T., Saito, Y., Yamamoto, T., Nishida, A., . . . Kokubun, S. (1998). Statistical analysis of the plasmoid evolution with Geotail observations. Journal of Geophysical Research: Space Physics, 103(A3), 4453-4465. doi:10.1029/97ja03240.

Jackman, C. M., Slavin, J. A., & Cowley, S. W. H. (2011). Cassini observations of plasmoid structure and dynamics: Implications for the role of magnetic reconnection in magnetospheric circulation at Saturn. Journal of Geophysical Research: Space Physics, 116(A10), n/a-n/a. doi:10.1029/2011ja016682.

Jackman, C. M., Slavin, J. A., Kivelson, M. G., Southwood, D. J., Achilleos, N., Thomsen, M. F., . . . Vogt, M. F. (2014). Saturn's dynamic magnetotail: A comprehensive magnetic field and plasma survey of plasmoids and traveling compression regions and their role in global magnetospheric dynamics. Journal of Geophysical Research: Space Physics, 119(7), 5465-5494. doi:10.1002/2013JA019388.

Jasinski, J. M., Arridge, C. S., Bader, A., Smith, A. W., Felici, M., Kinrade, J., . . . Murphy, N. (2019). Saturn's Open-Closed Field Line Boundary: A Cassini Electron Survey at Saturn's Magnetosphere. Journal of Geophysical Research: Space Physics, 124(12), 10018-10035. doi:10.1029/2019ja027090.

Kanani, S., Arridge, C. S., Jones, G., Fazakerley, A., McAndrews, H., Sergis, N., . . . Young, D. J. J. o. G. R. S. P. (2010). A new form of Saturn's magnetopause using a dynamic pressure balance model, based on in situ, multi-instrument Cassini measurements. 115(A6).

Kivelson, M. G., & Southwood, D. J. (2005). Dynamical consequences of two modes of centrifugal instability in Jupiter's outer magnetosphere. Journal of Geophysical Research, 110(A12). doi:10.1029/2005ja011176.

Machida, S., Ieda, A., Mukai, T., Saito, Y., & Nishida, A. (2000). Statistical visualization of Earth's magnetotail during substorms by means of multidimensional superposed epoch analysis with Geotail data. Journal of Geophysical Research: Space Physics, 105(A11), 25291-25303. doi:10.1029/2000ja900064.

Masters, A. (2017). Model-Based Assessments of Magnetic Reconnection and Kelvin-Helmholtz Instability at Jupiter's Magnetopause. Journal of Geophysical Research (Space Physics), 122, 11,154-111,174. doi:10.1002/2017JA024736.

Russell, C. T., & Elphic, R. C. (1978). Initial ISEE magnetometer results: magnetopause observations. Space Science Reviews, 22(6), 681-715. doi:10.1007/BF00212619.

Russell, C. T., & Elphic, R. C. (1979). ISEE observations of flux transfer events at the dayside magnetopause. Geophysical Research Letters, 6(1), 33-36. doi:10.1029/GL006i001p00033.

Slavin, J. A. (2003). Geotail observations of magnetic flux ropes in the plasma sheet. Journal of Geophysical Research, 108(A1). doi:10.1029/2002ja009557.

Smith, A., Jackman, C., & Thomsen, M. J. J. o. G. R. S. P. (2016). Magnetic reconnection in Saturn's magnetotail: A comprehensive magnetic field survey. 121(4), 2984-3005.

Tao, C., Kataoka, R., Fukunishi, H., Takahashi, Y., & Yokoyama, T. J. J. o. G. R. S. P. (2005). Magnetic field variations in the Jovian magnetotail induced by solar wind dynamic pressure enhancements. 110(A11).

Vasyliunas, V. M. (1983). Physics of the Jovian magnetosphere. 11. Plasma distribution and flow. In (pp. 395-453).

Vogt, M. F., Jackman, C. M., Slavin, J. A., Bunce, E. J., Cowley, S. W. H., Kivelson, M. G., & Khurana, K. K. (2014). Structure and statistical properties of plasmoids in Jupiter's magnetotail. Journal of Geophysical Research: Space Physics, 119(2), 821-843. doi:10.1002/2013JA019393.

Vourlidas, A., Lynch, B. J., Howard, R. A., & Li, Y. J. S. P. (2013). How many CMEs have flux ropes? Deciphering the signatures of shocks, flux ropes, and prominences in coronagraph observations of CMEs. 284(1), 179-201.

Yao, Z., Coates, A., Ray, L. C., Rae, I., Grodent, D., Jones, G. H., . . . Dunn, W. J. T. A. J. L. (2017). Corotating magnetic reconnection site in Saturn’s magnetosphere. 846(2), L25.

Yao, Z., Radioti, A., Grodent, D., Ray, L. C., Palmaerts, B., Sergis, N., . . . Roussos, E. J. J. o. G. R. S. P. (2018). Recurrent magnetic dipolarization at Saturn: Revealed by Cassini. 123(10), 8502-8517.

Young, D., Barraclough, B., Berthelier, J., Blanc, M., Burch, J., Coates, A., . . . Illiano, J. J. G. M.-A. G. U. (1998). Cassini plasma spectrometer investigation. 102, 237-242.

Zong, Q. G. (2004). Cluster observations of earthward flowing plasmoid in the tail. Geophysical Research Letters, 31(18). doi:10.1029/2004gl020692.

Figure 1.

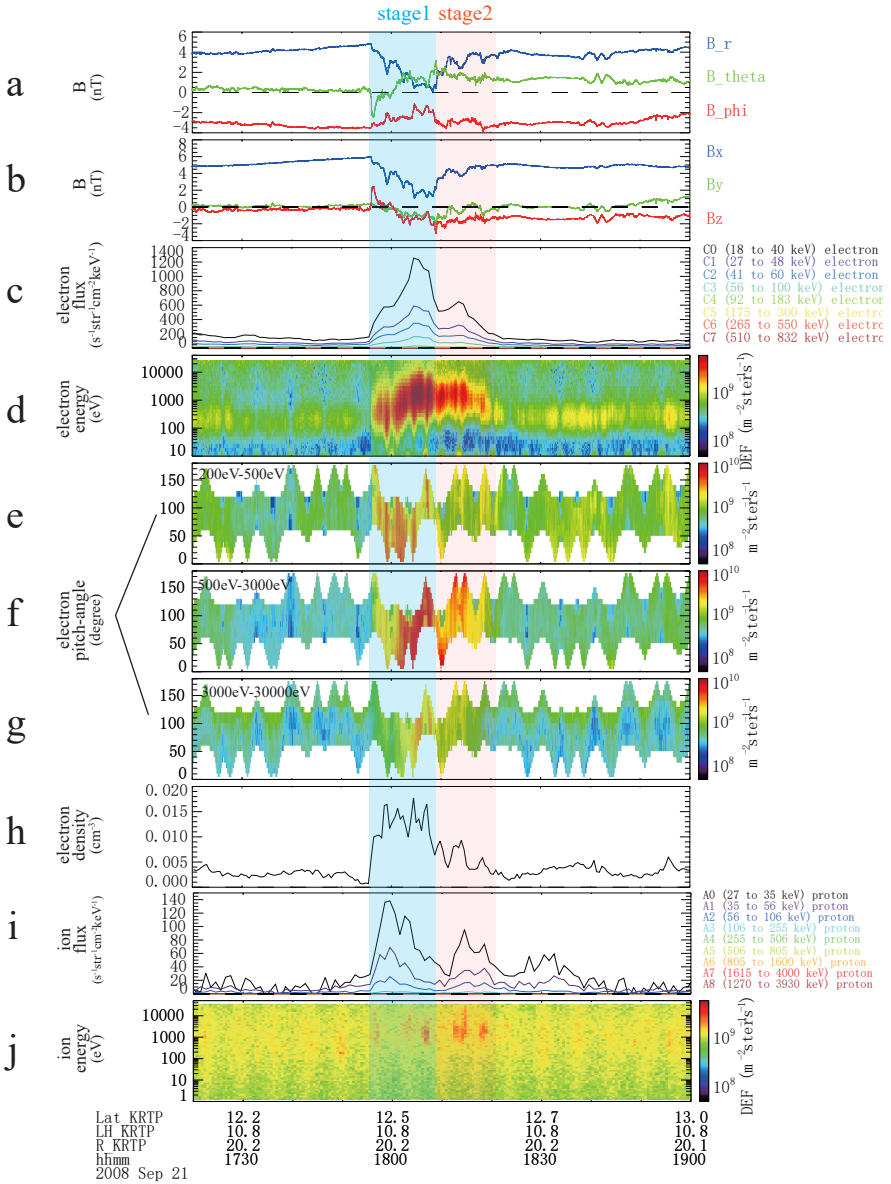
stage1
stage2
a
B (nT)
B_r
B_theta
B_phi
b
B (nT)
Bx
By
Bz
c
electron flux (s⁻¹str⁻¹cm⁻²keV⁻¹)
C0 (18 to 40 keV) electron
C1 (27 to 48 keV) electron
C2 (41 to 60 keV) electron
C3 (56 to 100 keV) electron
C4 (92 to 183 keV) electron
C5 (175 to 300 keV) electro
C6 (265 to 550 keV) electro
C7 (510 to 832 keV) electro
d
electron energy (eV)
DEF (m⁻²sterS⁻¹)
e
200eV-500eV
f
500eV-3000eV
g
3000eV-30000eV
electron pitch-angle (degree)
m⁻²sterS⁻¹
h
electron density (cm⁻³)
i
ion flux (s⁻¹str⁻¹cm⁻²keV⁻¹)
A0 (27 to 35 keV) proton
A1 (35 to 56 keV) proton
A2 (56 to 106 keV) proton
A3 (106 to 255 keV) proton
A4 (255 to 506 keV) proton
A5 (506 to 805 keV) proton
A6 (805 to 1600 keV) proton
A7 (1615 to 4000 keV) proton
A8 (1270 to 3930 keV) proton
j
ion energy (eV)
DEF (m⁻²sterS⁻¹)
Lat_KRTP 12.2 12.5 12.7 13.0
LH_KRTP 10.8 10.8 10.8 10.8
R_KRTP 20.2 20.2 20.2 20.1
hhmm 1730 1800 1830 1900
2008 Sep 21

Figure 2.

Dayside

Nightside

Event

Event/Background

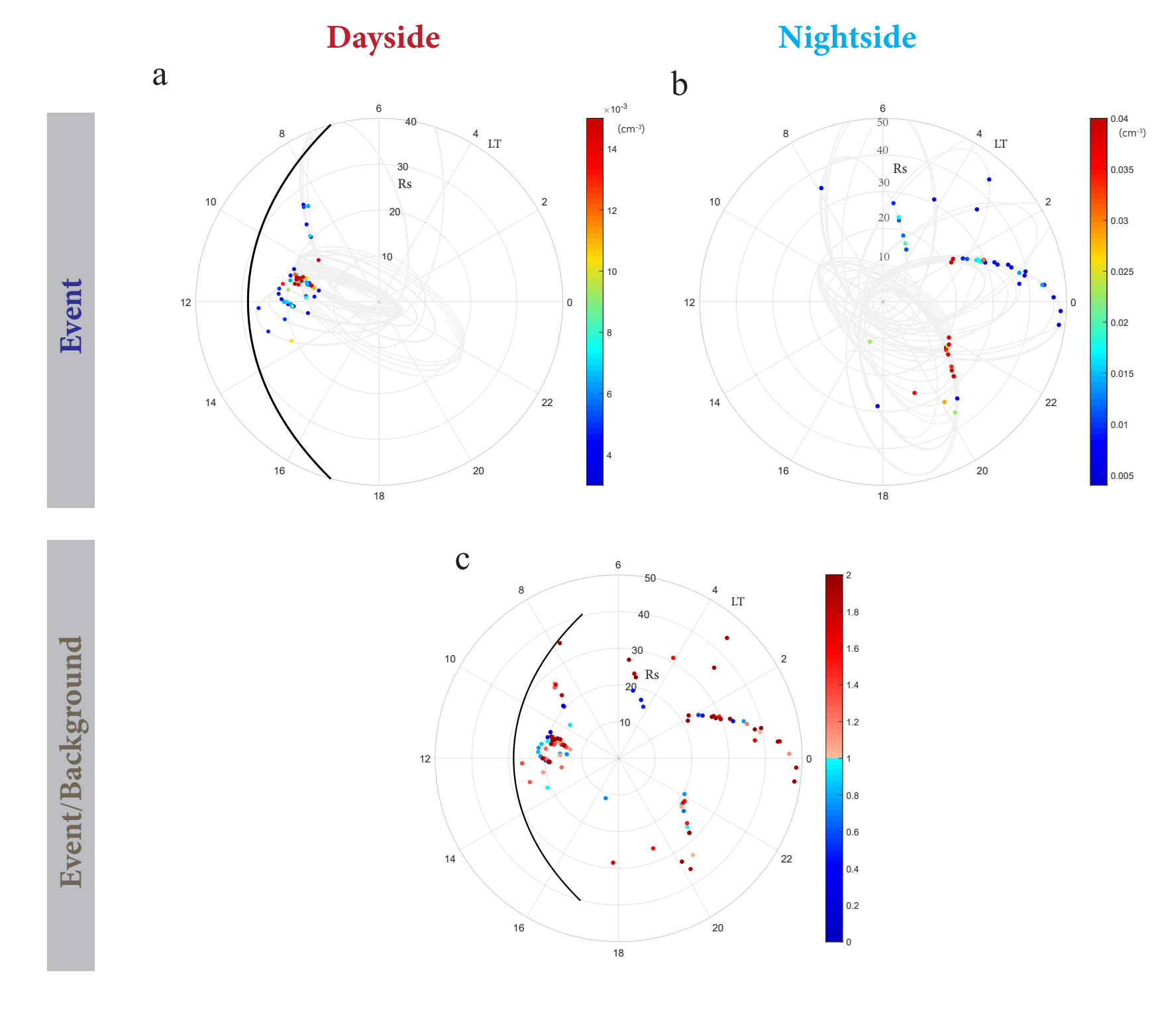

Figure 3.

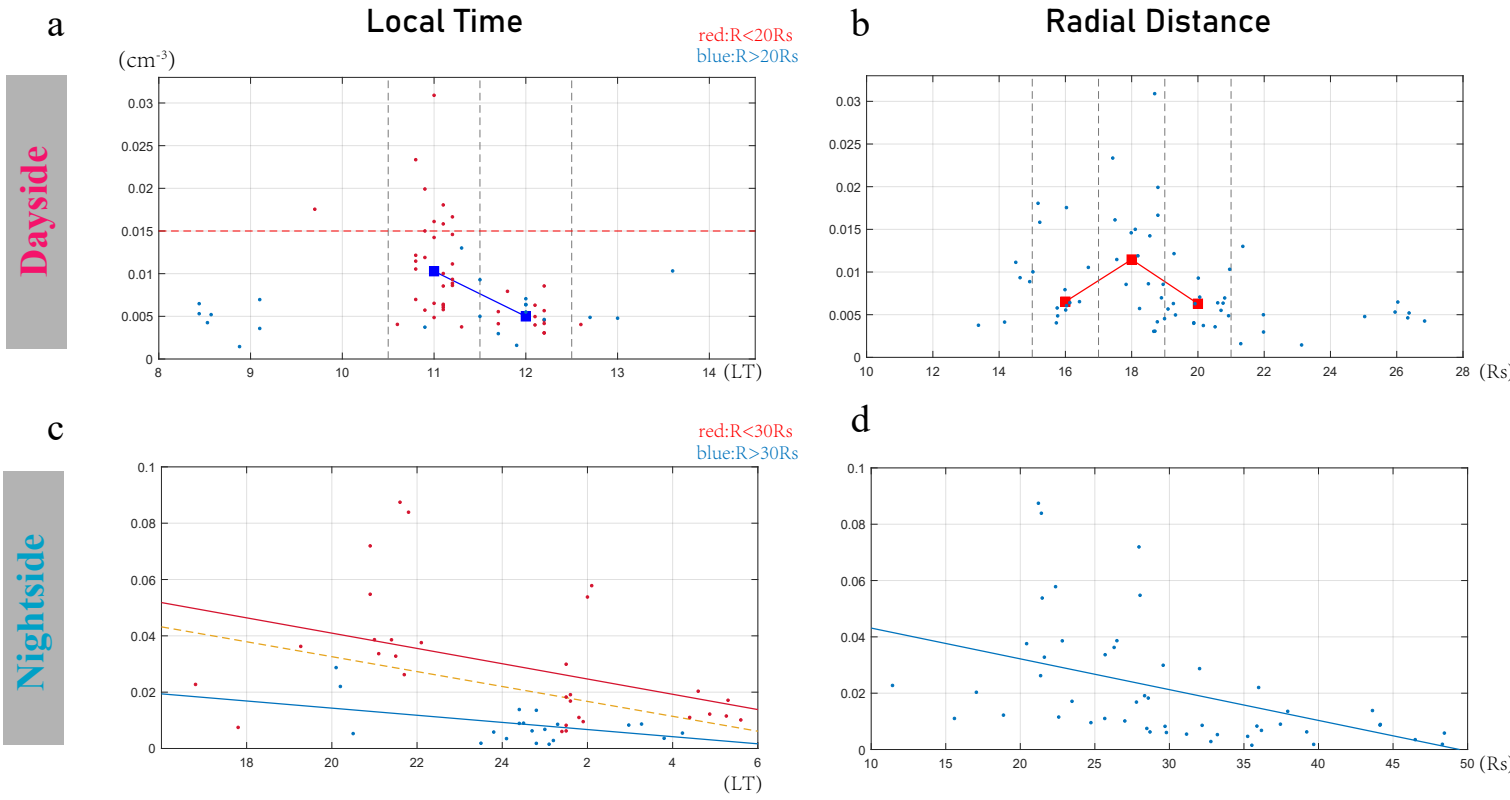
a
Local Time
b
Radial Distance
Dayside
red:R<20Rs
blue:R>20Rs
(cm-3)
0.03
0.025
0.02
0.015
0.01
0.005
0
8
9
10
11
12
13
14
(LT)
10
12
14
16
18
20
22
24
26
28
(Rs)
c
d
Nightside
red:R<30Rs
blue:R>30Rs
0.1
0.08
0.06
0.04
0.02
0
18
20
22
24
2
4
6
(LT)
10
15
20
25
30
35
40
45
50
(Rs)

Figure 4.

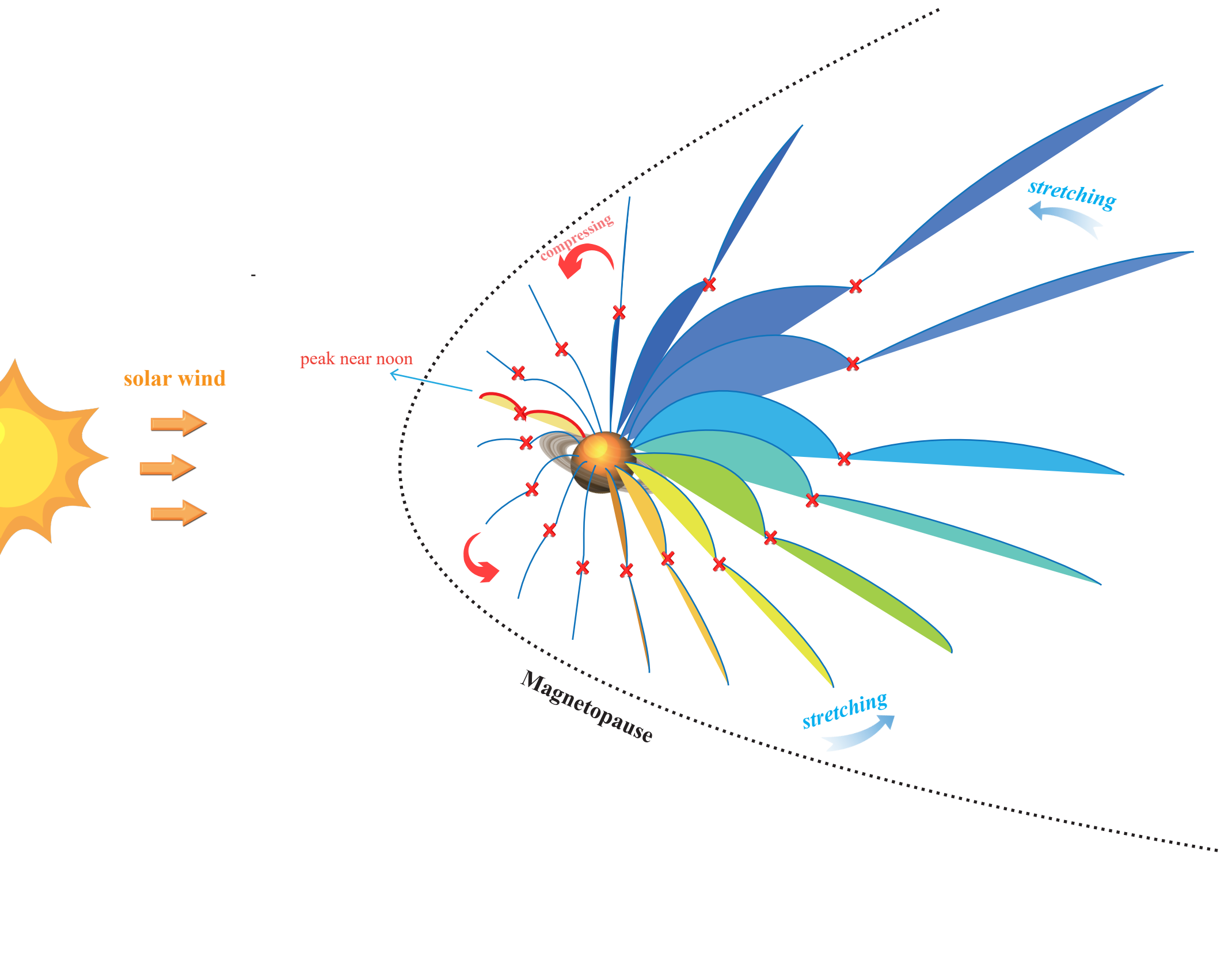
solar wind
peak near noon
compressing
stretching
stretching
Magnetopause